RESEARCH ARTICLE

Targeting DNA Damage Response Promotes Antitumor Immunity through STING-Mediated T-cell Activation in Small Cell Lung Cancer

Triparna Sen[1], B. Leticia Rodriguez[1], Limo Chen[1], Carminia M. Della Corte[1], Naoto Morikawa[1], Junya Fujimoto[2], Sandra Cristea[3,4], Thuyen Nguyen[3,4], Lixia Diao[5], Lerong Li[5], Youhong Fan[1], Yongbin Yang[1], Jing Wang[5], Bonnie S. Glisson[1], Ignacio I. Wistuba[2], Julien Sage[3,4], John V. Heymach[1,6], Don L. Gibbons[1,7], and Lauren A. Byers[1]

ABSTRACT Despite recent advances in the use of immunotherapy, only a minority of patients with small cell lung cancer (SCLC) respond to immune checkpoint blockade (ICB). Here, we show that targeting the DNA damage response (DDR) proteins PARP and checkpoint kinase 1 (CHK1) significantly increased protein and surface expression of PD-L1. PARP or CHK1 inhibition remarkably potentiated the antitumor effect of PD-L1 blockade and augmented cytotoxic T-cell infiltration in multiple immunocompetent SCLC *in vivo* models. $CD8^+$ T-cell depletion reversed the antitumor effect, demonstrating the role of $CD8^+$ T cells in combined DDR–PD-L1 blockade in SCLC. We further demonstrate that DDR inhibition activated the STING/TBK1/IRF3 innate immune pathway, leading to increased levels of chemokines such as CXCL10 and CCL5 that induced activation and function of cytotoxic T lymphocytes. Knockdown of *cGAS* and *STING* successfully reversed the antitumor effect of combined inhibition of DDR and PD-L1. Our results define previously unrecognized innate immune pathway–mediated immunomodulatory functions of DDR proteins and provide a rationale for combining PARP/CHK1 inhibitors and immunotherapies in SCLC.

SIGNIFICANCE: Our results define previously unrecognized immunomodulatory functions of DDR inhibitors and suggest that adding PARP or CHK1 inhibitors to ICB may enhance treatment efficacy in patients with SCLC. Furthermore, our study supports a role of innate immune STING pathway in DDR-mediated antitumor immunity in SCLC.

See related commentary by Hiatt and MacPherson, p. 584.

INTRODUCTION

In the past several years, immunotherapies that harness or enhance a patient's own immune system to target and kill cancer cells have been developed (1, 2). The most commonly used therapeutic approaches use antibodies against inhibitory signaling molecules expressed on tumor and immune cells. Common targets include the immune checkpoints PD-1, PD-L1, and CTLA4 (3). Since the first FDA approval of ipilimumab (anti-CTLA4) for melanoma, several such immune checkpoint blockade (ICB) agents have been approved for patients with advanced cancers, including non–small cell lung cancer (4–6).

Although ICB agents are very promising, their activity varies across different cancer types, and there is increasing evidence of primary and adaptive resistance to ICB in multiple cancer types (7). Thus, efforts are under way to develop new therapeutic strategies with novel drug combinations to enhance the antitumor efficacy of ICB. High mutational burden has been reported as a potential predictor of response to immunotherapy (8). However, despite having one of the highest mutational burdens, small cell lung cancer (SCLC) is often accompanied by relatively high immunosuppression with low levels of T-cell infiltration and reduced antigen presentation (9–11). Consistent with this, clinical trials investigating PD-1 or PD-L1 blockade in patients with SCLC have shown low overall response rates (12, 13).

Recent studies have demonstrated the potential of targeting the DNA damage response (DDR) pathway as a therapeutic strategy for SCLC (14–19), including drugs targeting PARP and checkpoint kinase 1 (CHK1). Several DDR inhibitors have been developed and are now either approved for the treatment of other cancers (e.g., PARP inhibitors) or in clinical trials (20). Although best known for its functions in repairing DNA damage and controlling the cell cycle, the DDR pathway has also been shown to be involved in the antitumor immune response (21). For example, the PARP inhibitor olaparib was recently reported to show a synergistic effect with PD-L1 blockade in triple-negative breast cancer in preclinical models (22). However, little is currently known regarding the mechanistic interactions between DDR targeting and response to ICB, as well as the immune-activating properties of DDR targeting.

In the current study, we identified a role of DDR targeting through CHK1 and PARP inhibition in modulating T-cell action via regulation of the innate immune response pathway. We found that pharmacologic inhibition of CHK1 or PARP increased levels of tumor-infiltrating T lymphocytes and synergized with anti–PD-L1 therapy in multiple SCLC models. Taken together, our results elucidate a mechanism of action for DDR inhibitors in antitumor immunity and

[1]Department of Thoracic/Head and Neck Medical Oncology, The University of Texas MD Anderson Cancer Center, Houston, Texas. [2]Department of Translational Molecular Pathology, The University of Texas MD Anderson Cancer Center, Houston, Texas. [3]Department of Pediatrics, Stanford University, Stanford, California. [4]Department of Genetics, Stanford University, Stanford, California. [5]Department of Bioinformatics and Computational Biology, The University of Texas MD Anderson Cancer Center, Houston, Texas. [6]Department of Cancer Biology, The University of Texas MD Anderson Cancer Center, Houston, Texas. [7]Department of Molecular and Cellular Oncology, The University of Texas MD Anderson Cancer Center, Houston, Texas.

Note: Supplementary data for this article are available at Cancer Discovery Online (http://cancerdiscovery.aacrjournals.org/).

Current address for Y. Yang: Department of Obstetrics and Gynecology, Shanghai General Hospital, Shanghai, China.

Corresponding Author: Lauren A. Byers, The University of Texas MD Anderson Cancer Center, 1515 Holcombe Boulevard, Unit 0432, Houston, TX 77030. Phone: 713-792-6363; Fax: 713-792-1220; E-mail: lbyers@mdanderson.org

doi: 10.1158/2159-8290.CD-18-1020

suggest that treatment with DDR inhibitors may increase the effectiveness of ICB in patients with SCLC.

RESULTS

DDR Inhibition Enhances PD-L1 Expression *In Vitro* and *In Vivo*

To determine the effect of DDR targeting on PD-L1 expression in SCLC models, we treated a panel of human SCLC cell lines with either a CHK1 inhibitor (prexasertib, 300 nmol/L) or a PARP inhibitor (olaparib, 1 μmol/L) for 72 hours and analyzed protein expression by reverse phase protein array (RPPA), immunoblot, and flow cytometry. DDR targeting significantly increased the total level of PD-L1 protein in all cell lines tested with prexasertib inducing the greatest PD-L1 fold change (up to 5-fold) and olaparib inducing an appreciable PD-L1 increase (up to 3-fold) as detected by RPPA ($P < 0.05$, Fig. 1A). The RPPA result was validated by immunoblot analysis, which further demonstrated PD-L1 upregulation upon DDR targeting in a time-dependent manner (Fig. 1B). As PD-L1 must be expressed on the cell surface for successful targeting, we then assayed cell surface PD-L1 expression by FACS. Cell surface PD-L1 levels significantly increased following treatment with either prexasertib or olaparib in a time-dependent manner in both human (Fig. 1C) and murine (RPP/mTmG; Fig. 1D) SCLC cell lines ($P < 0.05$ for all).

To confirm that PD-L1 upregulation is specifically due to inhibition of CHK1 or PARP and not an off-target effect of the inhibitors, we knocked down (KD) *CHEK1* or *PARP* in multiple SCLC cell lines. Consistent with pharmacologic inhibition, PD-L1 expression was substantially higher in *CHEK1* knockdown (Supplementary Fig. S1A) or *PARP* knockdown (Supplementary Fig. S1B) cells compared with the scrambled control. PD-L1 upregulation upon CHK1 targeting was further confirmed by treating cells with a second CHK1 inhibitor (LY2603618) in SCLC cell lines (Supplementary Fig. S1C).

Olaparib- and prexasertib-induced cytogenetic stress was evaluated using a micronuclei (MN) assay and represented as MN frequency, as demonstrated in Supplementary Fig. S1D and S1E. Treatment of SCLC cell lines H69, H446, and RPP/mTmG with prexasertib (1 μmol/L) or olaparib (10 μmol/L) for 24 hours led to a significant ($P < 0.001$) increase in MN frequency in treated samples. Representative micrographs using DAPI have been provided in Supplementary Fig. S1D, and number of MN/1,000 cells (H69, H446, and RPP/mTmG) is summarized in Supplementary Fig. S1E.

Given that PD-L1 expression was significantly enhanced following CHK1 inhibition (CHK1i), we hypothesized that CHK1i may induce an immune response in addition to direct antitumor effects in SCLC *in vivo* models and that CHK1i would be more effective in the immunocompetent (IC) setting. To test this possibility, we compared the effect of a low dose of prexasertib (12 mg/kg, b.i.d., 2 of 7 days, i.e., total 48 mg/kg/week), previously shown to cause growth delay but not tumor regression (18), on flank tumors grown in immunocompromised (nude) versus IC (B6129F1) mice. For these experiments, we used murine RPP/mTmG cells derived from a genetically engineered SCLC mouse with conditional loss of *Trp53, p130*, and *Rb1* (RPP; refs. 23, 24). The prexasertib-induced delay in tumor growth in the IC (B6129F1) model was significantly greater as compared with the immune-compromised (nude) model ($P < 0.001$), demonstrating the efficacy of CHK1 targeting in the context of an intact immune system (Fig. 1E). Prexasertib treatment induced PD-L1 protein expression in both the immunodeficient (ID) and IC *in vivo* model. However, a greater degree of PD-L1 upregulation was seen in the IC model (FC = 3.07) as compared with the ID model (FC = 1.28; Fig. 1F). The enhancement of PD-L1 expression in the IC model was further confirmed by immunoblot (Fig. 1G).

Next, we sought to determine whether CHK1i may induce changes in tumor-infiltrating immune cells in the lung microenvironment. We treated an IC model of SCLC, 4 months after Ad-CMV Cre intubation, bearing appreciable spontaneous RPP lung tumors (at least 50 tumors/lung; refs. 23, 24), with prexasertib at a dose that was previously shown to reduce tumor growth (10 mg/kg, b.i.d.; ref. 18). As predicted, prexasertib treatment increased PD-L1 protein expression in this model in a time-dependent manner (Supplementary Fig. S1F). At day 7, prexasertib-treated lung tumors had significantly more $CD3^+$ total T cells (Supplementary Fig. S1G) and $CD8^+$ cytotoxic T cells (Supplementary Fig. S1H), but decreased $CD4^+$ helper T cells (Supplementary Fig. S1I), PD-1^+/$TIM3^+$ exhausted T cells (Supplementary Fig. S1J), and $CD62L^+$ naïve T cells (Supplementary Fig. S1K) with a corresponding enhancement of $CD44^+$ memory/effector T-cell (Supplementary Fig. S1L) infiltration as compared with vehicle-treated tumors. The induction of PD-L1 expression, rapid tumor regression, and intratumoral immune infiltration following CHK1 targeting support a direct role for DDR modulation in regulating the immune microenvironment in these SCLC models.

CHK1i Augments Anti–PD-L1 Antibody–Induced Antitumor Immunity

As CHK1i alone is not sufficient to eradicate tumors despite reduced tumor growth, increased T-cell infiltration, and abrogated T-cell exhaustion *in vivo*, we next evaluated the ability of CHK1i to sensitize tumors to PD-L1 blockade. We treated B6129F1 IC flank RPP/mTmG tumor-bearing mice with prexasertib (10 mg/kg, 2/7days, b.i.d., days 1 and 2, i.e., total 40 mg/kg/week) and/or anti–PD-L1 (300 μg, 1/7 days, day 3) for 3 weeks ($n = 10$ per group; Supplementary Fig. S2A). Mice treated with anti–PD-L1 alone showed no antitumor response in this model and were sacrificed due to excessive tumor burden within 3 weeks. However, within 1 week, remarkable tumor regression was observed in the combination-treated group (Fig. 1H–J). Of the 10 mice treated with the combination of prexasertib and anti–PD-L1, 6 had a complete response (100% reduction).

Tumors were resected at day 21 (when available) and analyzed by multicolor flow cytometry for the changes in tumor-infiltrating lymphocytes (TIL; Supplementary Fig. S2B). Combination treatment with CHK1i and PD-L1 blockade significantly increased $CD3^+$ total T-cell infiltration (Fig. 2A and B; $P < 0.001$) and $CD8^+$ cytotoxic T-cell infiltration (Fig. 2C and D; $P < 0.001$). In addition, the single-agent prexasertib treatment increased the $CD44^+$ memory/effector T-cell population, which was further enhanced in the combination treatment ($P < 0.001$; Fig. 2E and F). Prexasertib + anti–PD-L1 treatment furthermore reduced the $CD62L^+$ naïve T-cell population ($P < 0.001$; Fig. 2E–G).

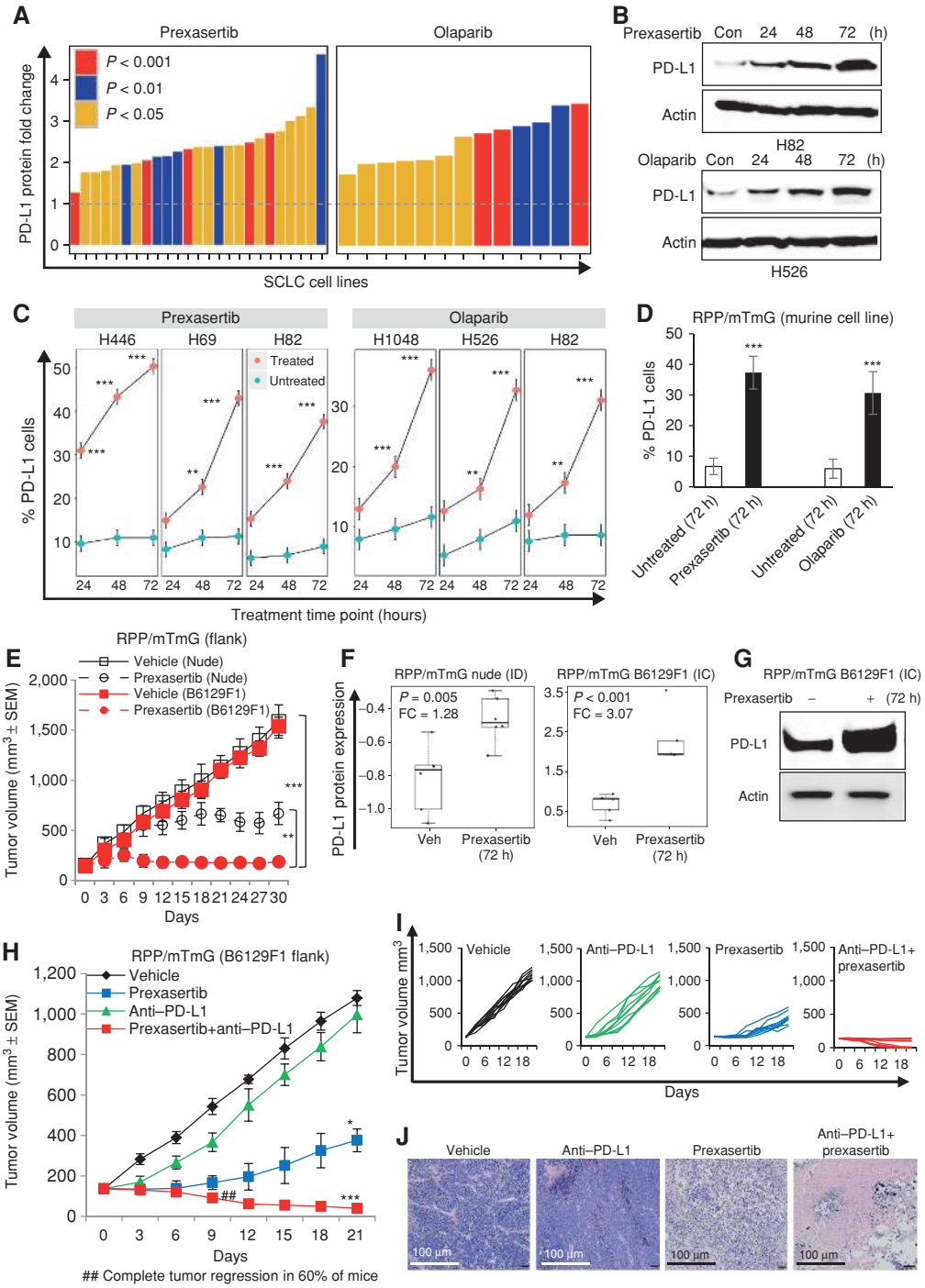

Figure 1. DDR inhibition enhances PD-L1 expression *in vitro* and *in vivo* and enhances antitumor response of anti–PD-L1 antibody in SCLC. **A–D,** DDR inhibition by targeting with small-molecule inhibitors of CHK1 (prexasertib) and PARP (olaparib) enhances the PD-L1 protein expression as measured by RPPA (**A**) and immunoblot analysis (**B**), and increases PD-L1 surface expression, as measured by flow cytometry in human (**C**) and murine (**D**) SCLC cell lines. **E,** Tumor growth curve of IC B6129F1 (red lines) model and immunocompromised nude (black lines) SCLC RPP/mTmG (flank) models treated with CHK1 inhibitor prexasertib (12 mg/kg, b.i.d., 2 of 7 days) for 30 days. Prexasertib showed enhanced antitumor efficacy in IC model (TC = 0.13; $P < 0.001$) as compared with immunocompromised model (T/C = 0.47; $P < 0.01$). **F,** Prexasertib treatment enhanced PD-L1 protein expression in SCLC tumors, with improved enhancement of PD-L1 expression in IC RPP/mTmG B6129F1 model (FC = 3.07; $P < 0.001$) as compared with ID RPP/mTmG nude model (FC = 1.28; $P = 0.005$). **G,** Immunoblot analysis confirms higher PD-L1 protein expression after prexasertib treatment in IC RPP/mTmG B6129F1 model. **H** and **I,** Tumor growth curves ± SEM (**H**) and for each RPP/mTmG B6129F1 mouse (**I**) from vehicle (black, $n = 10$, median tumor volume = 1,110 mm^3), prexasertib alone (10 mg/kg, 2 of 7 days, b.i.d., blue, $n = 10$, median tumor volume = 410 mm^3), anti–PD-L1 alone (300 μg, 1 of 7 days, i.p., green, $n = 10$, median tumor volume = 1,020 mm^3), and prexasertib + anti–PD-L1 (red, $n = 10$, median tumor volume = 40 mm^3). **J,** Representative hematoxylin and eosin (H&E) of the tumor sections from vehicle, prexasertib alone, anti–PD-L1 alone, and combination-treated group. All data represent at least three independent experiments. Mean ± SEM are plotted. In all plots, *, $P < 0.05$; **, $P < 0.01$; ***, $P < 0.001$; ns, not significant.

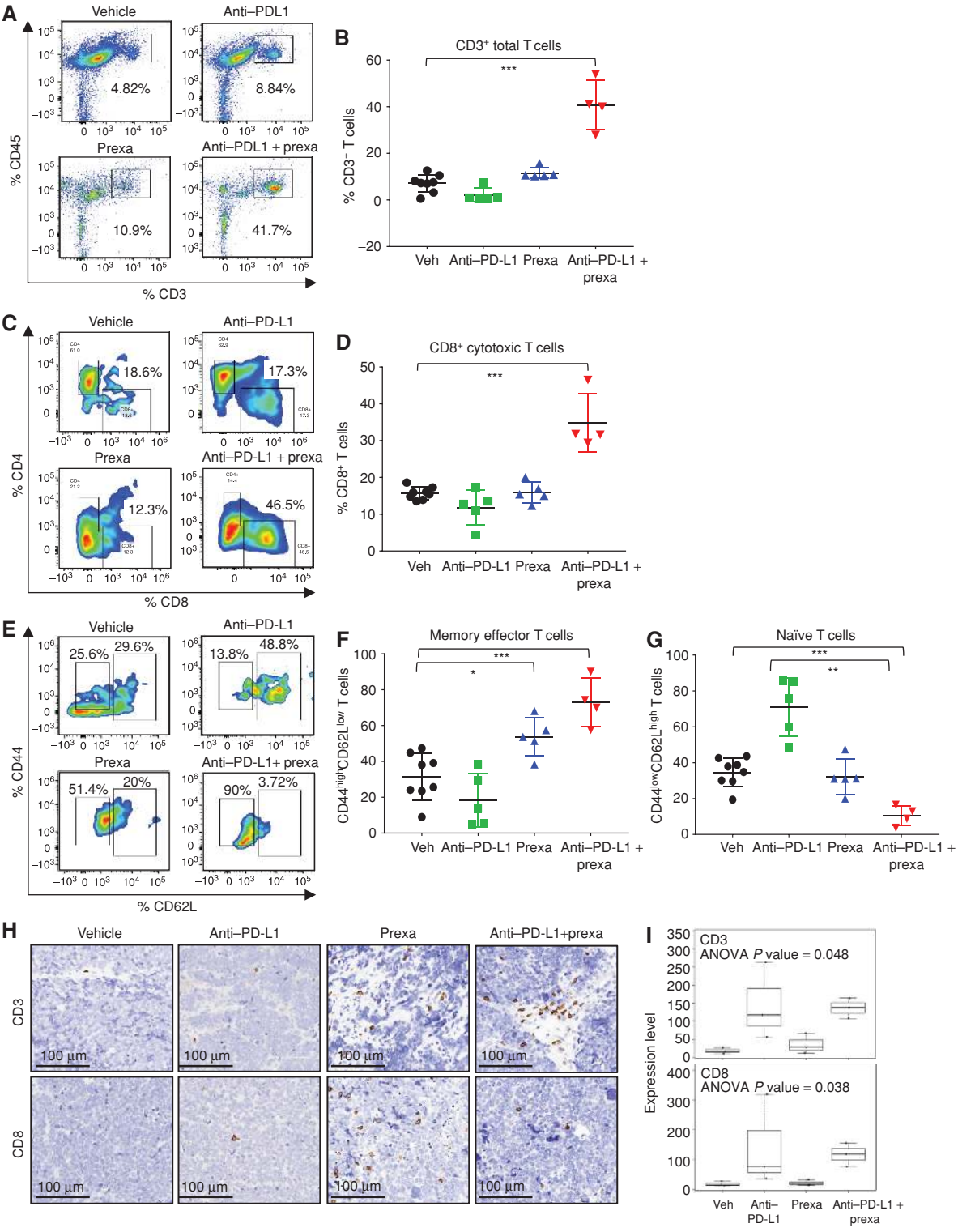

Figure 2. Analysis of immune infiltrates of tumors after CHK1i. **A–H,** SCLC tumors in Fig. 1H were harvested at day 21, the immune profiling was analyzed by FACS at the endpoint, and the representative plots and cumulative data for all the tumors are shown. FACS analysis of $CD3^+CD45^+$ total T cells (**A** and **B**), $CD3^+CD45^+CD8^+$ cytotoxic T cells (**C** and **D**), memory effector $CD8^+$ T cells: $CD45^+CD3^+CD8^+CD44^{hi}CD62L^{lo}$ (**E** and **F**), and naïve T cells $CD45^+CD3^+CD8^+CD44^{lo}CD62L^{hi}$ (**E** and **G**) from the endpoint primary tumors. The statistical summary is shown with ANOVA test. ns, no significance; *, $P < 0.05$; **, $P < 0.01$; ***, $P < 0.001$. **H** and **I,** The CD3 and CD8 IHC staining were performed in tumors from the resected tumors at day 21 (from Fig. 1H). Representative images of staining intensity are shown (**H**). The staining intensity and percentage of positive cells were analyzed and used to generate an H-score for each sample that passed quality control. Samples were stratified as $CD3/8^+$ (+1, +2, +3) and $CD3/8^-$ (0 and lower). The percentage of each expression pattern of CD3 and CD8 IHC staining was summarized and shown in the bar chart (**I**). prexa, prexasertib.

Prexasertib treatment alone or combination with PD-L1 blockade decreased CD4+ helper T-cell infiltration ($P < 0.001$; Supplementary Fig. S2C), the PD-1+/TIM3+ exhausted CD8+ T-cell population ($P < 0.001$; Supplementary Fig. S2D), and CD25+/FOXP3+ regulatory T-cell infiltration ($P < 0.001$; Supplementary Fig. S2E).

CD3 and CD8 IHC staining and scoring were performed on the resected tumors (from Fig. 1H). The IHC data confirm the flow cytometry observations with higher CD8 staining intensity and percentage of CD8+ cells in the prexasertib-treated group as compared with vehicle or anti–PD-L1 alone and further enhancement of this population in the anti–PD-L1 + prexasertib treatment tumors ($P < 0.05$; Fig. 2H and I). Therefore, CHK1 targeting by prexasertib significantly augments the antitumor immune response of anti–PD-L1 and causes cytotoxic T-cell infiltration and activation in an IC *in vivo* model of SCLC.

CD8+ T Cells Are Required for Antitumor Immunity Induced by CHK1i with or without Anti–PD-L1 Blockade

As CHK1i plus PD-L1 blockade resulted in complete tumor regression in 60% of the animals and FACS profiling of TILs from day 21 resected tumors revealed that prexasertib + anti–PD-L1 treatment induced CD8+ but not CD4+ T-cell infiltration, we hypothesized that the observed responses were mediated through CD8+ immune cell populations. To test whether intratumoral CD8+ T-cell suppression would reverse the antitumor effect of this combination, tumor-bearing mice (RPP/mTmG- flank) were treated with prexasertib ± anti–PD-L1 antibody in the presence of either control IgG or anti-CD8 antibody to immunodeplete CD8+ T cells (Supplementary Fig. S3A). CD8 depletion slightly enhanced tumor growth in the vehicle- and PD-L1 antibody–treated groups (Fig. 3A). In tumors treated with single-agent prexasertib or combined treatment of prexasertib and anti–PD-L1, we observed that depletion of CD8+ cytotoxic T cells significantly decreased the degree of tumor shrinkage relative to the control arms ($P < 0.001$; Fig. 3A; Supplementary Fig. S3B).

Flow cytometry confirmed successful intratumoral CD8+ T-cell depletion in tumors from all treatment arms ($P < 0.001$; Fig. 3B and C). In the CD8+ T cell–depleted models, we did not observe significant changes in the CD3+ total T-cell (Fig. 3D and E) or CD4+ helper T-cell infiltration following combination treatment as compared with the vehicle (Fig. 3C; Supplementary Fig. S3C). However, CD8+ T-cell depletion was associated with a higher percentage of exhausted T cells (PD-1+/TIM3+) in animals treated with the combination, as compared with the

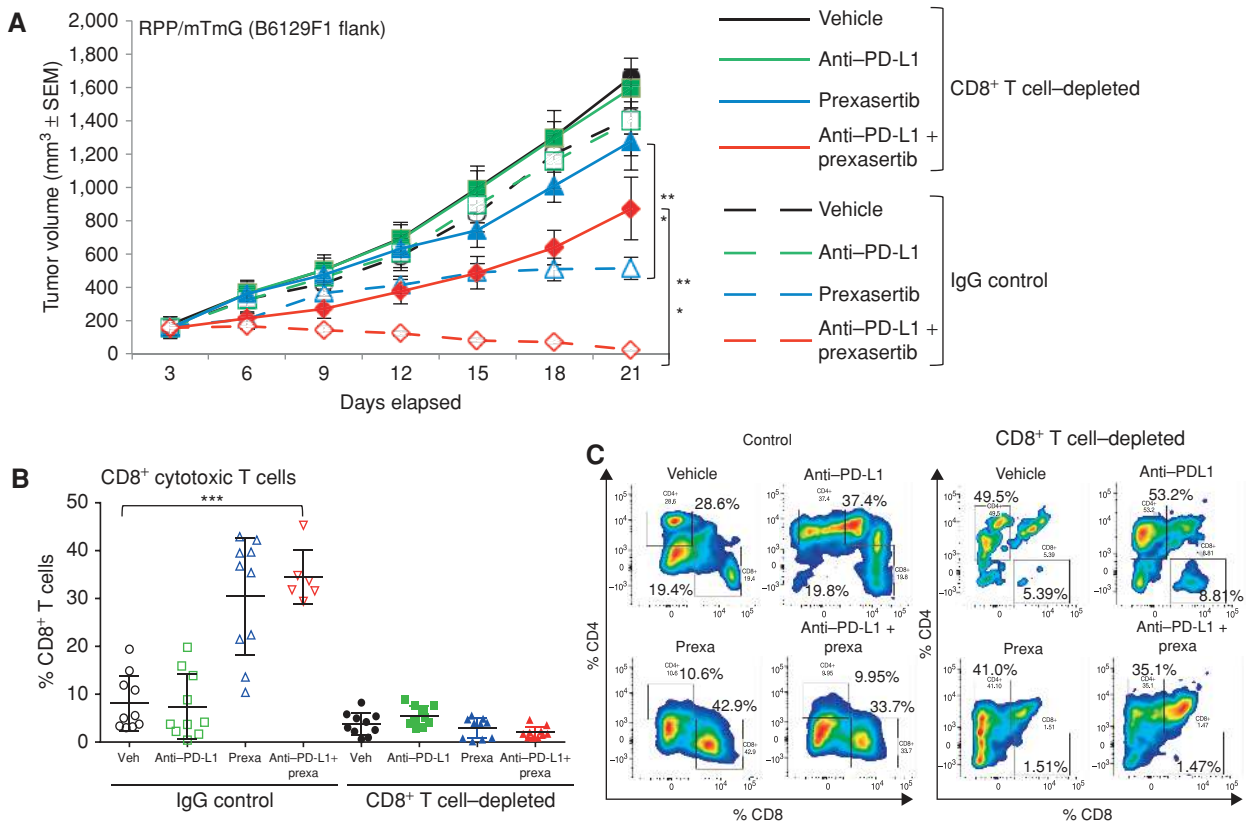

Figure 3. CD8+ T cells are required for antitumor immunity induced by CHK1i with or without anti–PD-L1 blockade. **A,** Tumor growth curves ±SEM from vehicle, prexasertib alone (10 mg/kg, 2 of 7 days, b.i.d.), anti–PD-L1 alone (300 μg, 1 of 7 days), and prexasertib + anti–PD-L1 treatment groups in RPP B6 mice in IgG control and CD8+ T cell–depleted (anti-CD8, 200 μg, 2 of 7 days) groups. **B** and **C,** CD8+ T cells measured by flow cytometric analysis in single-cell suspensions prepared from tumors ($n = 10$) in CD8+ T cell–depleted groups as compared with IgG control groups. The analysis was independently repeated at least 3 times. *t* test, $P < 0.0001$. prexa, prexasertib. (*continued on next page*)

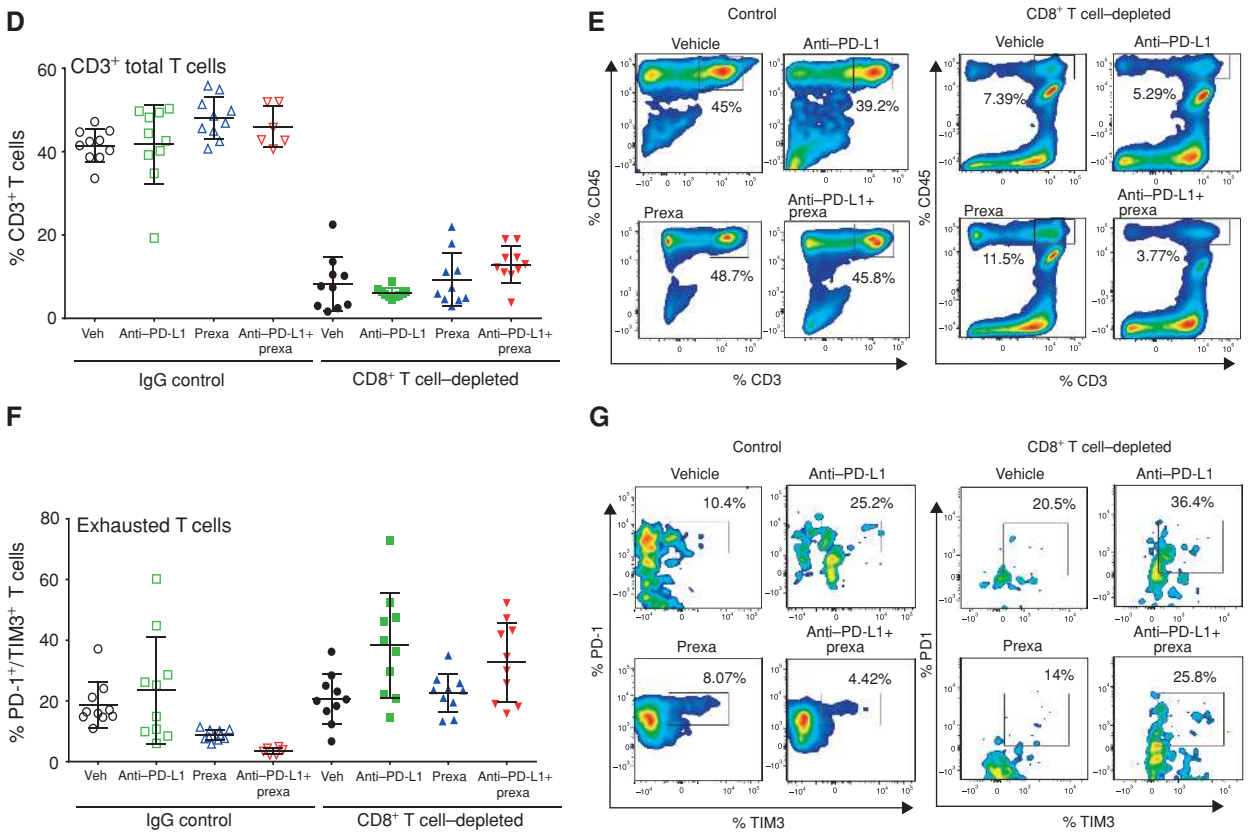

Figure 3. ***(Continued)*** **D–H,** SCLC tumors in **A** were harvested at day 21, the immune profiling was analyzed by FACS at the endpoint, and the representative plots and cumulative data for all the tumors are shown. FACS analysis of $CD3^+CD45^+$ total T cells (**D** and **E**) and exhausted $CD8^+$ T cells $CD45^+CD3^+CD8^+PD\text{-}1^+TIM3^+$ (**F** and **G**) from the endpoint primary tumors. The statistical summary is shown with ANOVA test. ***, $P < 0.001$.

CD8-intact group (Fig. 3F and G). $CD8^+$ T-cell depletion also did not cause any significant changes in the naïve ($CD44^{medium}$/$CD62L^{hi}$) or memory/effector ($CD44^{hi}$/$CD62L^{lo}$) T cells (Supplementary Fig. S3D and S3E). Thus, we conclude that CHK1i greatly potentiates the effects of PD-L1 blockade *in vivo* through a $CD8^+$ T cell–induced antitumor immune response.

PARP Inhibition Augments Anti–PD-L1 Antibody–Induced Antitumor Immunity

Based on the findings above, we next tested whether targeting a second important DNA repair protein, PARP, could enhance the antitumor immunity of anti–PD-L1 antibody, similar to the effect we observed with CHK1i. We have previously shown that PARP is overexpressed in SCLC tumors (14) and that PARP inhibition has activity in preclinical models (15, 25), and recent clinical trials have demonstrated clinical benefit from PARP inhibitors in some patients with SCLC (16, 19). As described above, we observed a significant increase in PD-L1 levels following PARP inhibition or knockdown in SCLC cell lines in culture (Fig. 1A–C).

To test the effect of PARP targeting on response to ICB and the immune microenvironment, we treated an IC SCLC model (RPP) with an FDA-approved PARP inhibitor (olaparib, 50 mg/kg, 5 of 7 days) and/or anti–PD-L1 (10 mg/kg, 3 of 7 days; Supplementary Fig. S4A). Single-agent olaparib treatment had no significant antitumor activity, and consistent with the previous observation, anti–PD-L1 alone had no antitumor effect in these models (Fig. 4A). However, we observed striking tumor regressions in animals treated with the combination of olaparib and anti–PD-L1. All animals had a complete tumor regression as early as day 7, and the effect was sustained until day 80 (Fig. 4A and B). Consistent with these findings, the overall survival of the olaparib + anti–PD-L1–treated group was significantly higher than the IgG-, anti–PD-L1-, or olaparib-treated groups ($P < 0.001$; Fig. 4B).

Due to total tumor regression in the olaparib + anti–PD-L1–treated group in the IC RPP flank model (Fig. 4A and B), there were no resectable tumors for downstream analyses. Thus, we tested a lower dose of olaparib and collected tumors from all treatment arms on day 21 to determine changes in the immune microenvironment. In this experiment, we treated established RPP flank tumors in IC B6129F1 mice with olaparib (50 mg/kg, days 1–4 of 7 days) and/or anti–PD-L1 (300 μg, 1 of 7 days) for 3 weeks (Supplementary Fig. S4B). As expected, neither single-agent olaparib nor anti–PD-L1 antibody demonstrated significant antitumor benefit as compared with IgG vehicle control (Supplementary Fig. S4C and S4D). However, even at a lower dose, the combination treatment led to significant delay in tumor

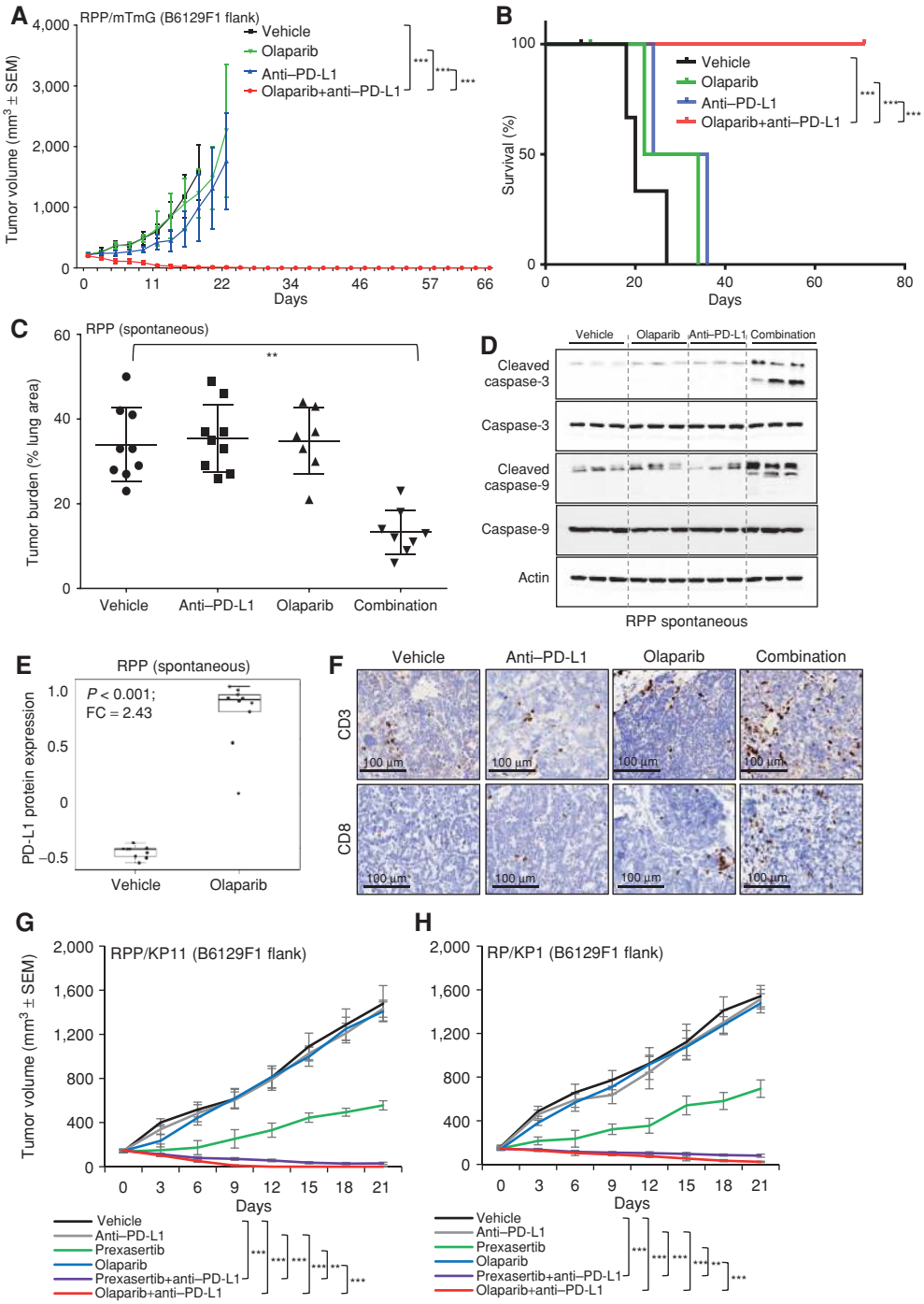

Figure 4. PARP inhibition augments anti-PD-L1 antibody-induced antitumor immunity. **A** and **B,** B6129F1 mice were injected with murine RPP derived from SCLC in a genetically engineered mice with conditional loss of *Trp53*, *p130*, and *Rb1*. Tumor volume changes (mean ± SEM; error bars; **A**) and survival of mice (**B**) treated with IgG (10 mg/kg, 3 of 7 days), anti-PD-L1 (10 mg/kg, 3 of 7 days), olaparib (50 mg/kg, 5 of 7 days), and the combination ($n = 5$ per group) up to 80 days. For the survival curve, the *P* value was established by the Mantel–Cox test. **C,** Quantification of tumor burden as a percentage of lung area in *Trp53/Rb1/p130*-knockout mice treated with vehicle IgG, olaparib (50 mg/kg, 5 of 7 days), anti-PD-L1 (300 μg, 1 of 7 days), or combination (one random lung section quantified per mouse). **D,** Immunoblot analysis of tumors treated with vehicle, olaparib, anti-PD-L1, and combination resected at day 21. Analysis performed for a panel of apoptosis markers, pro and cleaved caspase-3 and 9. Actin was used a loading control. **E,** Olaparib treatment enhanced PD-L1 protein expression in RPP spontaneous tumors as measured by RPPA analysis (FC = 2.43; $P < 0.001$). **F,** The CD3 and CD8 IHC staining were performed in tumors from the resected tumors from **C**. Representative images of staining intensity are shown. The staining intensity and percentage of positive cells were analyzed and used to generate an H-score for each sample that passed quality control. Samples were stratified as CD3/8$^+$ (+1, +2, +3) and CD3/8$^-$ (0 and lower). **G** and **H,** B6129F1 mice were injected with an additional cell line derived from RPP model (KP11) and from RP model (derived from SCLC in genetically engineered mice with conditional loss of *Trp53* and *Rb1*), KP1. Tumor volume changes (mean ± SEM; error bars) of KP11 (**G**) and KP1 (**H**) treated with IgG, anti-PD-L1 (300 μg, 1/7), olaparib (50 mg/kg, 5 of 7 days), prexasertib (10 mg/kg, 2 of 7 days, b.i.d.), combination of olaparib and anti-PD-L1, and combination of prexasertib and anti-PD-L1 ($n = 6$ per group) treated for 21 days. In all plots, *, $P < 0.05$; **, $P < 0.01$; ***, $P < 0.001$; ns, not significant.

growth (Supplementary Fig. S4C and S4D). Following olaparib treatment, we again observed a significant increase in tumor PD-L1 protein expression by RPPA analysis ($P < 0.001$, FC = 1.47; Supplementary Fig. S4E) which was confirmed by immunoblot analysis (Supplementary Fig. S4F).

To investigate the effects of this combination in the endogenous lung microenvironment, we tested olaparib and anti–PD-L1 in the spontaneous RPP genetically engineered mouse model (GEMM) mode of SCLC. We further performed histologic analysis of the pretreatment tumors at 4 months after Ad-CMV-Cre administration to ascertain tumor burden. As expected from prior experience with this model, we observed appreciable tumor burden at this time by analysis of hematoxylin and eosin (H&E)–stained sections (Supplementary Fig. S5A). The mice were randomized into groups based on their baseline tumor burden (as measured by luciferase imaging represented in Supplementary Fig. S5B) to ensure comparable tumor burdens between treatment groups. Based on prior experience with this model (18), we treated spontaneous RPP tumor–bearing mice with olaparib (50 mg/kg, days 1–4 of 7 days) and/or anti–PD-L1 (300 μg, 1 of 7 days) for 3 weeks (treatment schema, Supplementary Fig. S4B) starting about 4 months after administration with Ad-CMV-Cre, when all mice had more than 50 SCLC tumors growing in their lungs. When tumor burden was quantified after 3 weeks of treatment (Fig. 4C), single-agent olaparib or anti–PD-L1 did not cause any appreciable change in the tumor burden as compared with the IgG control mice. However, olaparib + anti–PD-L1–treated tumors occupied a significantly smaller fraction of the total lung area and were fewer in number, suggestive of tumor regression (Fig. 4C; $P < 0.001$). We further performed an immunoblot analysis of tumor lysates resected from the lungs for a panel of apoptosis markers (cleaved caspase 3 and 9) to investigate tumor cell killing in the animals treated with the combination regimen. In agreement with the changes in tumor volume, we observed no appreciable change in cleaved caspase 3 or 9 after olaparib or anti–PD-L1 single-agent treatments (Fig. 4D). However, there was a noticeable increase in the expression of cleaved caspase 3 and 9 in the tumors treated with the combination of olaparib and anti–PD-L1, thus confirming tumor cell killing with this treatment (Fig. 4D). Moreover, olaparib treatment appreciably increased PD-L1 protein expression compared with vehicle-treated animals ($P < 0.001$; Fig. 4E). IHC staining of lung sections demonstrated no change in CD8-positive cells in the olaparib-treated group as compared with vehicle or anti–PD-L1 alone. However, we observed a significantly higher CD8 staining intensity and percentage of $CD8^+$ cells in anti–PD-L1 + olaparib–treated group (Fig. 4F).

Immune profiling by flow cytometry of resected lung tumors showed no change in the $CD3^+$ total T-cell, $CD4^+$ helper T-cell, or $CD8^+$ cytotoxic T-cell infiltration upon single-agent olaparib or anti–PD-L1 treatment (Supplementary Fig. S5C–S5G). However, there was a significant increase in the $CD3^+$ total T-cell and $CD8^+$ cytotoxic T-cell and decrease in the $CD4^+$ helper T-cell infiltration in the olaparib + anti–PD-L1 treatment group (Supplementary Fig. S5C–S5G). Interestingly, we observed an increase in the $PD\text{-}1^+/TIM3^+$ exhausted T cells and $CD25^+/FOXP3^+$ T-regulatory cells upon treatment with single-agent olaparib or anti–PD-L1 antibody (Supplementary Fig. S5H–S5K). However, consistent with the antitumor response, treatment with olaparib + anti–PD-L1 antibody decreased the percentage of tumor-infiltrating $PD\text{-}1^+/TIM3^+$ exhausted $CD8^+$ T cells and $CD25^+/FOXP3^+$ $CD4^+$ T-regulatory cells (Supplementary Fig. S5H–S5K).

We further performed immune profiling of flank tumors shown in Supplementary Fig. S4C and S4D to see whether consistent changes were induced versus the endogenous lung tumors. Single-agent olaparib or anti–PD-L1 antibody did not change $CD3^+$ total T-cell or $CD8^+$ cytotoxic T-cell and only minimally decreased $CD4^+$ helper T-cell infiltration as compared with IgG control (Supplementary Fig. S6A–S6E). However, treatment with the combination of olaparib and anti–PD-L1 led to a significant increase in the $CD3^+$ total T-cell or $CD8^+$ cytotoxic T-cell, and decrease in $CD4^+$ helper T-cell, infiltration as compared with IgG control (Supplementary Fig. S6A–S6E). Furthermore, we observed either single-agent olaparib or anti–PD-L1 treatment increased $CD25^+FOXP3^+$ CD4 T-regulatory and $PD\text{-}1^+/TIM3^+$ $CD8^+$ exhausted T-cell infiltration with a significant decrease in these populations upon combined inhibition with olaparib and anti–PD-L1 (Supplementary Fig. S6F–S6I).

Thus, in summary, although PARP targeting by olaparib alone did not significantly change $CD8^+$ cytotoxic T-cell infiltration, combined inhibition of PARP and PD-L1 caused remarkable tumor regressions and increased infiltration of $CD8^+$ cytotoxic T cells, and a decrease in the exhausted and regulatory T cells.

To further confirm that the synergistic antitumor effect of combined DDR–PD-L1 targeting is not model-specific, we investigated the effect of this combination in additional SCLC models. For this, we selected an additional RPP model (KP11 cell line) and a *Trp53*$^{f/f}$, *Rb1*$^{f/f}$ (*Trp53*$^{-/-}$/*Rb1*$^{-/-}$) double-knockout RP model (KP1 cell line). We treated B6129F1-IC flank RPP/KP11 (Fig. 4G) and RP/KP1 (Fig. 4H) tumor-bearing mice with prexasertib (10 mg/kg, 2/7days, b.i.d., days 1 and 2) or olaparib (50 mg/kg, 5 of 7 days) with or without anti–PD-L1 (300 μg, 1/7 days) for 3 weeks ($n = 5$ per group). As expected, anti–PD-L1 had no antitumor benefit in either the KP11 or KP1 model (Fig. 4G and H). Similar to the effect observed in the RPP/mTmG model, we saw no change in tumor growth with olaparib treatment in either the KP11 or KP1 model (Fig. 4G and H). Single-agent prexasertib, however, showed significant delay in tumor growth in both models (Fig. 4G and H). Notably, in agreement with previous models, combined targeting of PD-L1 and either CHK1 or PARP led to remarkable antitumor effect in these models. In KP11, by day 21, we observed complete tumor regression in 2 of 5 animals when treated with prexasertib + anti–PD-L1 antibody, and complete regression in 5 of 5 animals when treated with olaparib + anti–PD-L1 antibody. In KP1, by day 21, we observed complete tumor regression in 1 of 5 animals when treated with prexasertib + anti–PD-L1 antibody and complete regression in 3 of 5 animals when treated with olaparib + anti–PD-L1 antibody. These observations clearly demonstrated that the synergistic antitumor benefit of combined DDR and PD-L1 blockade is not model-specific in SCLC.

Antitumor Immune Response after DDR Targeting Is Mediated via the STING–TBK1–IRF3 Pathway in SCLC

Based on the rapid antitumor immune response we observed following DDR inhibitor treatment, we hypothesized that the immune modulation induced by DDR targeting may occur, at least in part, through activation of

the innate immune system. Previous reports have shown that DNA damage that arises from cytotoxic agents can activate the STING pathway, an innate immune pathway activated by cytoplasmic DNA (26–30). Cyclic guanosine monophosphate (GMP)–adenosine monophosphate (AMP) synthase (cGAS) is a DNA sensor that triggers innate immune responses through production of the second messenger, cyclic GMP–AMP (cGAMP), which binds and activates the adaptor protein STING (26–30). cGAMP binding to STING triggers phosphorylation of IRF3 via TBK1, and IRF3 then translocates to the nucleus to trigger transcription of inflammatory genes.

To test whether the STING pathway was activated in SCLC models in response to the DDR inhibitors prexasertib and olaparib (31), we treated SCLC cell lines and tumors with prexasertib and olaparib and assessed STING pathway activation by transcriptomic and proteomic assays. We observed the presence of cytosolic DNA after treatment with prexasertib and olaparib, which is indicative of DNA damage (Supplementary Fig. S7A). We next found that treatment with prexasertib for 24 and 72 hours led to a time-dependent activation of the STING pathway including pSTING_S366, pTBK1_S172, cGAS, and pIRF3_S396 in multiple human SCLC cell lines (H82, H69, and H841; Fig. 5A). STING pathway

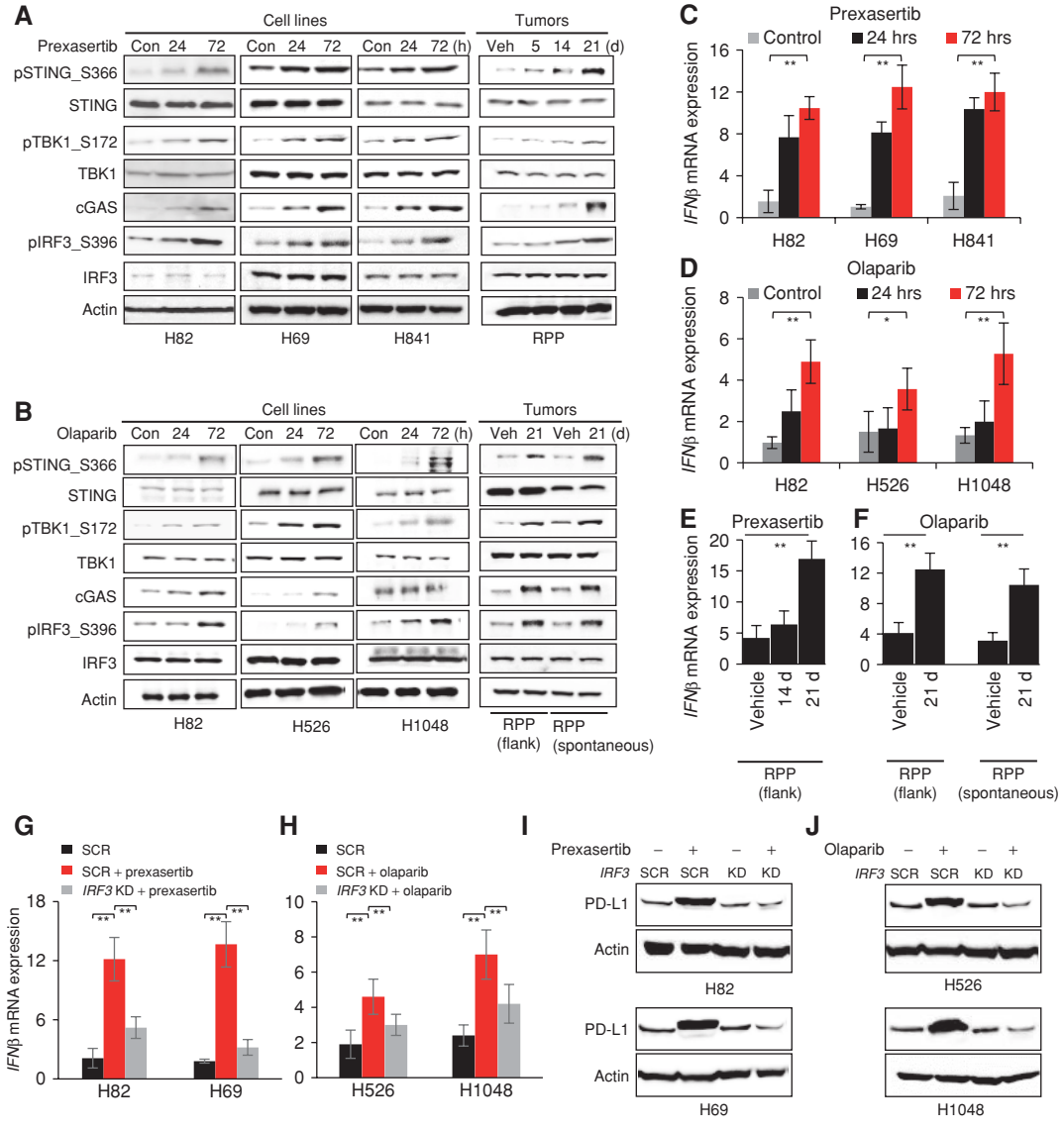

Figure 5. Antitumor immune response after DDR targeting is mediated via the STING–TBK1–IRF3 pathway in SCLC. **A** and **B,** Immunoblots of markers in the STING pathway including total and phospho (p) STING (S366), total and phospho TBK1 (S172), cGAS, total and phospho IRF3 (S396) in lysates collected from SCLC cell lines and tumors treated with prexasertib (**A**) or olaparib (**B**). Actin served as a loading control. **C** and **D,** qPCR measurement of *IFNβ* mRNA expression in SCLC cell lines 24 and 72 hours after prexasertib (**C**) and olaparib (**D**) treatment. **E** and **F,** qPCR measurement of *IFNβ* mRNA expression in SCLC tumor models after treatment with prexasertib in RPP flank model (**E**) and olaparib in RPP flank and spontaneous (**F**) SCLC *in vivo* models. **G** and **H,** qPCR measurement of *IFNβ* mRNA expression 72 hours after treatment with prexasertib (**G**) and olaparib (**H**). *IRF3* expression was KD 24 hours prior to drug treatment using siRNA targeting *IRF3*. A scrambled siRNA control (SCR) is included. All data representative of mean ± SD. *, $P < 0.05$; **, $P < 0.01$; ***, $P < 0.001$. **I** and **J,** Immunoblot of PD-L1 in SCLC cells treated with prexasertib (**I**) and olaparib (**J**; 72 hours). *IRF3* expression was KD in all cells 24 hours prior to drug treatment using siRNA targeting *IRF3*. A scrambled siRNA control (SCR) is included.

activation was also observed in flank murine RPP tumor samples collected on days 5, 14, and 21 of prexasertib treatment (Fig. 5A). A similar STING pathway activation was observed upon olaparib treatment in multiple SCLC cell lines (H82, H526, and H1048) where PARP targeting enhanced expression of pSTING_S366, pTBK1_S172, cGAS, and pIRF3_S396 in a time-dependent manner (Fig. 5B). Activation of the STING pathway was also observed in olaparib-treated murine RPP tumors collected from flank RPP and spontaneous lung RPP models 21 days after treatment (Fig. 5B). In contrast, when SCLC cell lines were treated with a drug that does not induce DDR, paclitaxel (PTX; 10 and 20 μmol/L for 48 hours), we did not observe any change in the expression of PD-L1 or any of the main STING pathway proteins (pSTING_S366 and cGAS; Supplementary Fig. S7B). Phosphohistone H3 was assessed to demonstrate ongoing cell division (Supplementary Fig. S7B). These data indicate that, although DDR inhibition causes release of cytosolic DNA which further triggers STING pathway activation, no such effect is observed with a drug that does not induce DDR.

IRF3 has been previously identified as a transcription factor for type I interferon genes, particularly *IFNβ* (32, 33). Because DDR targeting led to the activation of IRF3, we predicted that the increase in IRF3 levels after DDR targeting would enhance the mRNA expression of *IFNβ*. Prexasertib and olaparib treatment caused significant increases in the mRNA expression of *IFNβ* in multiple SCLC cell lines in a time-dependent manner (Fig. 5C and D). Similar enhancement of *IFNβ* expression upon treatment with prexasertib (Fig. 5E) or olaparib (Fig. 5F) was observed in SCLC RPP-mTmG *in vivo* tumors. In contrast, treatment with PTX (10 and 20 μmol/L for 48 hours) did not cause any appreciable change in the mRNA expression of *IFNβ* (Supplementary Fig. S7C), further demonstrating that the STING-mediated activation of type I interferon is DDR targeting–mediated. Moreover, prexasertib and olaparib treatment caused significant increases in *IFNβ* expression in RP-KP1 and RPP-KP11 tumors at day 21 (Supplementary Fig. S7D). Notably, siRNA-mediated *IRF3* knockdown, as confirmed by immunoblot analysis (Supplementary Fig. S7E), abrogated the prexasertib-mediated (Fig. 5G) or olaparib-mediated (Fig. 5H) upregulation of *IFNβ* mRNA expression. Because the type I interferon pathway can regulate PD-L1 expression, we next investigated the role of IRF3 on PD-L1 expression. Interestingly, *IRF3* knockdown abrogated the increase in PD-L1 protein expression after prexasertib (Fig. 5I) or olaparib (Fig. 5J) treatment in SCLC models, supporting a direct role of IRF3-mediated type 1 interferon genes in regulating PD-L1 in SCLC.

Next, we aimed to determine the extent to which the synergistic antitumor effect of combined DDR–PD-L1 blockade is mediated through tumor-cell cGAS-mediated STING activation. To accomplish this, we depleted either cGAS or STING in SCLC RPP/mTmG cells. The knockdown efficiency was determined by Western blot analysis (Supplementary Fig. S7F, *cGAS*; Supplementary Fig. S7G, *STING*). The cGAS- or STING-depleted tumor cells were then injected into IC mice and treated with either prexasertib (10 mg/kg, b.i.d., 2/7 days) or olaparib (50 mg/kg, 5/7 days) with or without PD-L1 (300 μg, 1/7 days) blockade ($n = 5$/group). In tumors harboring knockdown of *cGAS* or *STING*, we observed a significantly decreased degree of tumor shrinkage relative to control arms (Fig. 6A and B). Contrary to parental control (Con) and scrambled control (SCR) tumors, all *cGAS* and *STING* KD tumors progressed even with combined CHK1i/PARPi and PD-L1 blockade ($P < 0.001$), confirming the vital role of the cGAS/STING pathway in DDR-mediated antitumor response in SCLC models. We collected tumors from animals treated with either vehicle or olaparib at the end of the 3 weeks and investigated the expression of *cGAS* and *STING* in control versus knockdown tumors. As predicted, we observed an increase in cGAS and no detectable changes in total STING after olaparib treatment in control cells (Fig. 6C and D). Furthermore, we observed undetectable levels of cGAS and STING before and after olaparib treatment in cGAS and STING knockdown tumors, respectively (Fig. 6C and D).

IRF3, a major effector of the STING/TBK1 signaling pathway, has been reported to regulate the expression of chemokines such as CXCL10 and CCL5. Because CXCL10 and CCL5 are key mediators for the chemotaxis of $CD8^+$ T lymphocytes, and CXCL10 and CCL5 overexpression is associated with the presence of $CD8^+$ T lymphocytes in melanoma and gastric and colorectal cancers (34, 35), we next investigated the previously unexplored link between DDR targeting and chemokine expression in SCLC. Prexasertib and olaparib treatment caused significant upregulation of *CXCL10* and *CCL5* mRNA expression in multiple SCLC cell line (Fig. 7A) and tumor (Fig. 7B) models ($P < 0.001$ for all). siRNA-mediated knockdown of *STING* (Supplementary Fig. S7H) resulted in significantly reduced expression of *CXCL10* (Fig. 7C) and *CCL5* (Fig. 7D) after prexasertib or olaparib treatment in multiple SCLC models.

In summary, we observed that DDR targeting by CHK1 or PARP inhibition induces DNA damage and activates the STING–TBK1–IRF3 pathway in SCLC models, leading to the expression of PD-L1 and type 1 interferon IFNβ. Furthermore, DDR targeting leads to the higher expression of chemokines CXCL10 and CCL5 in SCLC, dependent on STING pathway activation. This activation leads to the recruitment of $CD8^+$ T lymphocytes and antitumor immunity, as summarized in our working model (Fig. 7E).

DISCUSSION

DDR inhibition and ICB are both therapeutic strategies under preclinical and clinical development for patients with SCLC. Here, we report a previously unexplored role of DDR pathway targeting in regulating antitumor immune response in SCLC models, specifically that inhibition of DDR proteins such as CHK1 and PARP potentiates the antitumor immune response of PD-L1 blockade through T cell–mediated effects. This effect is mediated through activation of the STING/TBK1/IRF3 innate immune response pathway, which ultimately enhances expression of the type 1 interferon gene *IFNβ* and downstream chemokines such as CXCL10 and CCL5 to induce activation and function of cytotoxic T lymphocytes. When combined with ICB, e.g., anti–PD-L1 antibody, DDR targeting demonstrates significant antitumor effect, suggesting that these combinations may be valuable clinically to overcome primary and adaptive resistance to ICB in SCLC.

Despite significant enthusiasm for immunotherapy approaches in lung cancer, only a minority of patients with

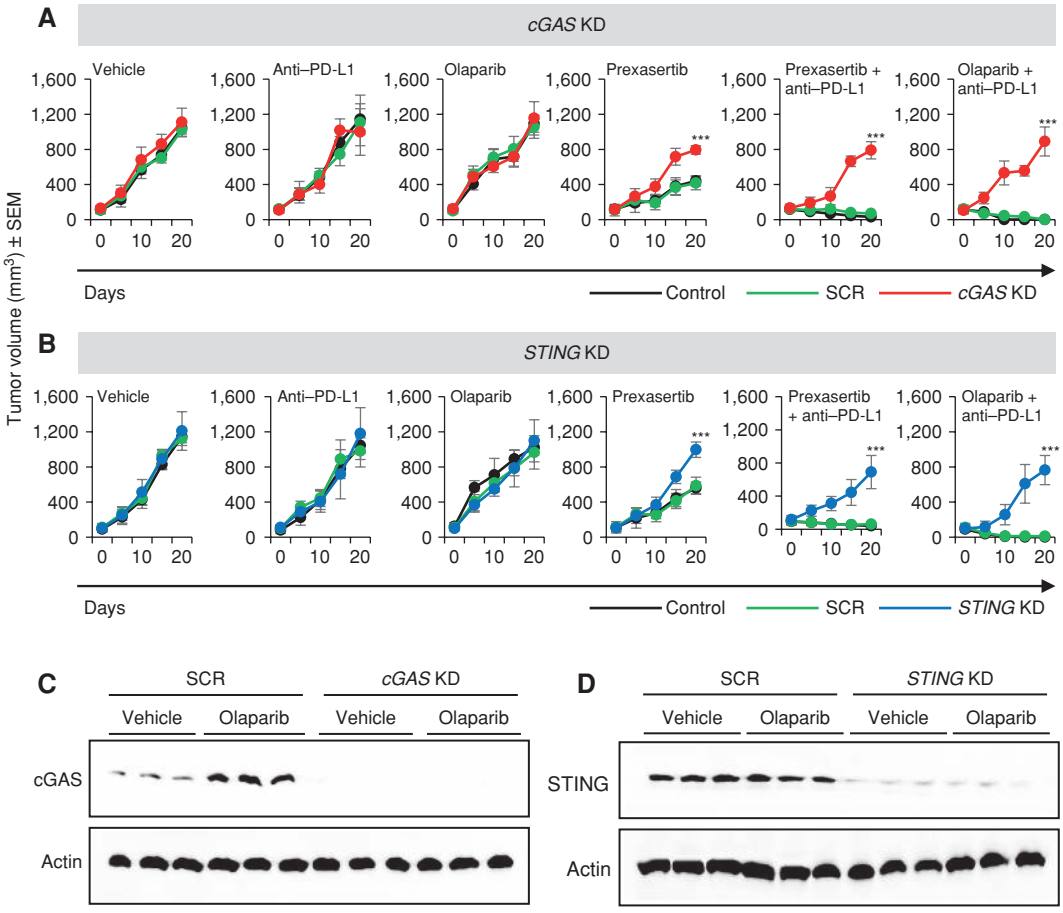

Figure 6. Knockdown of *cGAS* and *STING* reverses the antitumor effect of combined DDR and PD-L1 blockade *in vivo*. **A** and **B,** Tumor growth curves ±SEM from vehicle, prexasertib alone (10 mg/kg, 2 of 7 days, b.i.d.), olaparib alone (50 mg/kg, 5 of 7 days), anti–PD-L1 alone (300 μg, 1 of 7 days), prexasertib + anti–PD-L1, and olaparib + anti–PD-L1 treatment groups in B6129 mice with RPP/mTmG parental control (Con), scrambled (SCR), *cGAS* knockdown (**A**) and *STING* knockdown (**B**) groups. **C** and **D,** Immunoblot analysis for cGAS and STING of tumors resected at the end of treatment (day 21) from SCR or *cGAS* and *STING* knockdown models treated with either vehicle or olaparib. Actin used as loading control. In all plots, *, $P < 0.05$; **, $P < 0.01$; ***, $P < 0.001$; ns, not significant.

SCLC respond to anti–PD-1 monotherapy or anti–PD-1/anti-CTLA4 combination (approximately 10% with monotherapy and 23% with the combination; refs. 36, 37). Despite having one of the highest mutational burdens among solid tumors, SCLC paradoxically shows lower expression of PD-L1 and relatively immunosuppressed phenotypes with low levels of infiltrating T cells and reduced antigen presentation (38). Recent clinical data illustrating that tumors with defective DDR, such as microsatellite instability–high or mismatch repair–deficient tumors, predict improved response to anti–PD-1 therapy support the hypothesis that the addition of a DDR inhibitor to anti–PD-1 therapy may significantly enhance response rates and outcomes (39). Furthermore, some recent reports have demonstrated PD-L1 upregulation by DNA damage (40). However, it is not known to what extent pharmacologic inhibitors of DDR targets may enhance ICB response or the mechanism through which this occurs.

SCLC exhibits ubiquitous loss in two key regulators of the DNA damage and cell-cycle checkpoint pathway, *TP53* and *RB1,* which leads to high genomic instability and replication stress (20, 41). Therefore, we hypothesized that targeting this inherent DNA repair vulnerability with DDR inhibitors to promote an immune response may be an effective strategy to achieve a quick and sustained antitumor immune response by potentiating the effect of a combination ICB regimen. Because the response with DDR targeting occurs quickly, we hypothesized that in SCLC the activation of the innate immune response machinery may lead to DDR-mediated immune activation.

Previous studies have reported the presence of cytosolic DNA post-S phase damage, and additional evidence suggests that cells may actively export DNA fragments from the nucleus, possibly to prevent misincorporation into genomic DNA (42). In turn, the presence of cytosolic DNA in the absence of efficient DNA damage repair triggers cGAS-mediated innate immune response. Here, we demonstrated increased cytosolic DNA following treatment with either DDR inhibitor (prexasertib or olaparib) *in vitro*. We further observed that targeting CHK1 or PARP leads to the activation of the STING/cGAS/TBK1 pathway, thus upregulating PD-L1 expression. *IRF3* knockdown studies confirmed the role of the transcription factor in the DDR targeting–mediated antitumor immune response and PD-L1 regulation in SCLC. We further observed upregulation of *IFNβ* after DDR targeting in SCLC, which could be an indirect mechanism

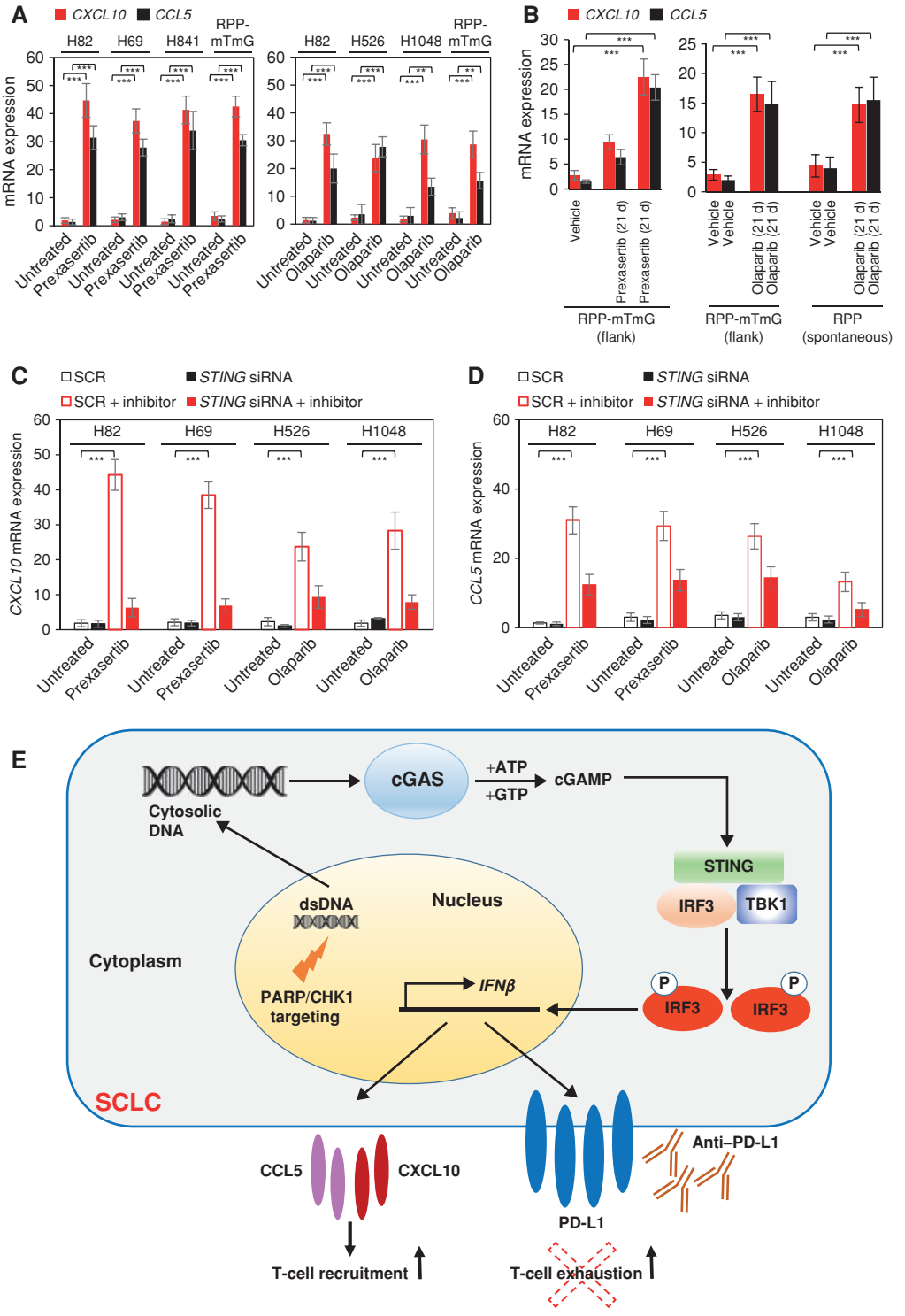

Figure 7. Role of STING pathway in DDR targeting–dependent chemokine expression. **A** and **B,** RT-qPCR measurement of chemokines *CXCL10* (red) and *CCL5* (black) mRNA extracted from SCLC cell lines treated with prexasertib (left) and olaparib (right) for 72 hours (**A**) and tumors treated with prexasertib (RPP flank, left) and olaparib (RPP flank and spontaneous model, right) after 1 cycle of treatment (**B**). **C** and **D,** qPCR measurement of *CXCL10* (**C**) and *CCL5* (**D**) mRNA 72 hours following knockdown of *STING* using siRNA in SCLC cell lines normalized to a nontargeting scrambled control (SCR) after prexasertib and olaparib (inhibitor) treatment. In all plots, *, $P < 0.05$; **, $P < 0.01$; ***, $P < 0.001$; ns, not significant. **E,** Model for STING pathway activation in response to DDR targeting in SCLC. In the proposed model, targeting the DDR proteins PARP and CHK1 with the small-molecule inhibitors prexasertib and olaparib leads to cytosolic DNA in SCLC models. The cytosolic DNA is then recognized by cGAS, which leads to activation of the STING/TBK1/IRF3 pathway. IRF activation leads to increased expression of *IFNβ* and enhanced expression of the chemokines CXCL10 and CCL5. STING pathway activation and increased chemokine expression lead to increased PD-L1 expression and T-cell recruitment in SCLC models. Finally, DDR cotargeting leads to enhanced antitumor immunity in SCLC models.

of regulating PD-L1 levels in these tumors. Moreover, in our models we demonstrated significant increase in the expression of the chemokines CXCL10 and CCL5 after DDR inhibitor treatment. The abrogation of the expression after STING knockdown indicates the role of these chemokines in STING–TBK1–RF3-mediated antitumor immune response. It is not known to what extent increased tumor mutation burden induced by DDR targeting may also contribute to enhancing ICB response. However, based on our observations here with tumor shrinkage starting soon after treatment (often seen within days), the rapid innate response—rather than changes in neoantigens—seems likely to be a more important contributor at least in the initial response. Also, because the mouse tumors have previously been shown to have low mutation burden (41), future studies to monitor the effects of DDR inhibition in patients with SCLC will be valuable to provide further insights into the effect of DDR-mediated STING activation and immune response.

In summary, the effects of CHK1 and PARP on DNA damage repair and cell-cycle progression lead to T-cell recruitment and enhanced effector cell function in SCLC tumors, mediated by the activation of the innate immune response pathway STING/TBK1/IRF3 and increased *IFNβ*. Activation of the STING-mediated pathway is responsible for chemokine production in response to DNA damage *in vitro,* thereby resulting in increased immunogenicity of the otherwise immunosuppressed tumors. The pathway also leads to the upregulation of PD-L1 expression. Expression of PD-L1 is associated with tumors deficient in DNA damage repair, and we, for the first time, provide rationale for investigating the role of immunotherapy in the context of DDR targeting in SCLC. Moreover, our results demonstrating the remarkable efficacy of the combination of PD-L1 blockade with PARP or CHK1 inhibition provide a strong scientific rationale for combining these modalities in clinical trials for patients with SCLC. Further studies will be necessary to carefully interrogate the contribution, if any, of the neoantigen load and other immune cell populations, such as natural killer cells (43), during DDR-mediated T-cell activation. Because prexasertib, olaparib, and other PARP inhibitors are already in clinical trials for SCLC, we expect that these findings have the potential for rapid translation into the clinic.

METHODS

Cell Lines and Characterization

SCLC human-derived cell lines were obtained from the American Type Culture Collection (ATCC) or Sigma-Aldrich between the years 2011 and 2015.

The GEMM-derived SCLC cell lines were established from a genetically engineered mouse model, derived from either a double-knockout *Trp53*$^{f/f}$, *Rb1*$^{f/f}$ (*p53*$^{-/-}$/*Rb1*$^{-/-}$) (RP-KP1) model or a triple-knockout model of SCLC, which closely mimics the human disease and has a *Trp53*$^{f/f}$, *Rb12*$^{f/f}$, *Rb1*$^{f/f}$ (*p53*$^{-/-}$/*p130*$^{-/-}$/*Rb1*$^{-/-}$) (RPP/mTmG; RPP/KP11) allelic genotype with a ROSA26R reporter. Complete cell line information is provided in Supplementary Table S1.

All cell lines were tested and authenticated by short tandem repeat profiling (DNA fingerprinting) within 6 months of the study and routinely tested for *Mycoplasma* species before any experiments were performed.

Chemical Compounds

LY2603618 was obtained from Selleckchem.com. Prexasertib and olaparib were manufactured by MD Anderson's Institute for Applied Chemical Science. All compounds were dissolved in dimethyl sulfoxide for *in vitro* treatments.

DNA Fingerprinting to Confirm Cell Line Identity

DNA from 5 to 6 × 10^6 cells was isolated using a QIAamp DNA mini kit (Qiagen), following the manufacturer's protocol. The isolated DNA was eluted in elution buffer (100 μL; Buffer AE, Qiagen). The concentration of the DNA and its purity was measured by NanoDrop. Cell line authentication was done by using DNA (50 ng) for DNA fingerprint analysis of short tandem repeat profiling (PowerPlex 1.2, Promega). Fingerprinting results for each cell line were compared with reference fingerprints provided by Dr. Minna or the ATCC.

Mice

For the syngeneic mouse model, 6-week-old IC female B6129F1 (Taconic) were used. These animals were maintained in accordance with the Institutional Animal Care and Use Committee of The University of Texas MD Anderson Cancer Center and the National Institutes of Health Guide for the Care and Use of Laboratory Animals.

The spontaneous GEMM mice were maintained according to practices prescribed by the NIH at the Stanford Research Animal Facility, which is accredited by the Association for the Assessment and Accreditation of Laboratory Animal Care. The RPP conditional knockout mouse model induced by intratracheal administration of Ad-CMV-Cre for SCLC has been described previously (24).

Establishment of Syngeneic Flank Tumors and Studies in B6129F1 Mice

The mouse SCLC cell line was derived from tumors isolated from RPP mice (RPP-mTmG; RPP-KP11 cell lines) or RP mice (RP-KP1). For subcutaneous injections, 0.5 × 10^6 mouse SCLC (mTmG) cells were injected into one flank of each mouse with Matrigel (1:1; BD Biosciences).

Treatment Schedule of SCLC In Vivo Models

Mice with mouse SCLC tumors received one of the following treatments: (1) vehicle; (2) anti–PD-L1 (9G2; BioXcell; 300 μg) once per week; (3) prexasertib (10 mg/kg twice daily) 2 consecutive days per week; or (4) combination of anti–PD-L1 (300 μg) once per week and prexasertib (10 mg/kg twice daily) 2 consecutive days per week.

For the PARP inhibitor experiments, mice received one of the following treatments: (1) vehicle; (2) olaparib (50 mg/kg daily) 4 times per week; (3) anti–PD-L1 (300 μg) once per week; or (4) combination of olaparib and anti–PD-L1.

Tumors were collected for single-cell preparation for flow cytometry, snap-frozen in liquid nitrogen for protein isolation, or fixed in 4% paraformaldehyde in PBS at 4°C and processed for paraffin histologic analysis. Sections of paraffin-embedded tissues (4 μm) were stained with H&E and collected for IHC.

Development of Spontaneous SCLC Tumors and Dosing Schedule

Mice were maintained according to practices prescribed by the NIH at the Stanford Research Animal Facility, which is accredited by the Association for the Assessment and Accreditation of Laboratory Animal Care. The RPP triple-knockout mouse model for SCLC has been previously described. The mice were bred onto a mixed genetic background composed of C57BL/6, 129/SvJ, and 129/SvOla. Tumors

were induced in young adult mice by intratracheal instillation of 4×10^7 plaque-forming units of adenovirus expressing Cre recombinase (Ad-Cre; Baylor College of Medicine, Houston, TX).

To determine baseline amount of tumors before treatment, mice were injected with luciferin (Biosynth), anesthetized with isoflurane (VetOne), and dorsal hair shaved between the head and stomach. The mice were imaged for luciferase luminescence using an IVIS CCD camera. The mice were separated into treatment groups to ensure all cohorts had comparable levels of luminescence, which is proportional to the amount of tumors in the mouse.

Treatment was initiated 4 months after Ad-Cre delivery, at a time when infected mice had developed more than 50 independent lesions. The CHK1 inhibitor prexasertib (10 mg/kg, b.i.d.) was injected subcutaneously at the nape of the neck every 12 hours for 3 days in a row, for 1 week (i.e., 10 mg/kg, twice daily, days 1, 2, and 3 of a 7-day cycle, for one cycle). For olaparib, the mice were treated either with olaparib (50 mg/kg, 4/7) and/or with anti–PD-L1 (300 μg, 1/7). Control mice were injected with IgG control. The lung tumors were collected and processed for single-cell isolation.

Real-Time PCR

Real-time PCR was done using SYBR Select Master Mix (Life Technologies, cat# 4472908) according to the manufacturer's protocol. The primers were purchased from Sigma; the details of the primers are given in Supplementary Table S2. Triplicate PCR reactions were run on ABI (7500 Fast Real Time PCR System) according to the manufacturer's instructions. The comparative Ct method using the average 2ΔΔCT value for each set of triplicates was used, and the average of the biological replicates was calculated. Negative controls were included for every primer set, and GAPDH was used as the positive control.

Flow Cytometry

Single-cell suspensions were prepared and stained according to standard protocols for flow cytometry with antibodies listed in Supplementary Table S3. For intracellular staining, cells were fixed and permeabilized with BD Cytofix/Cytoperm (BD Biosciences). The data were acquired on a Fortessa or Calibur platform (BD Biosciences) and analyzed with FlowJo software (version 7.6; Tree Star). For analyzing the abundance and the function of $CD4^+$ or $CD8^+$ TILs, single-cell suspensions were prepared from tumors and inguinal lymph nodes and stained; the staining of inguinal lymph node cells was used as the reference of lymphocyte gating, then $CD3^+$ cells were gated, and then $CD4^+$ or $CD8^+$ population was analyzed.

For details on cell culture, transient knockdown of *CHEK1, PARP, IRF3,* and *TMEM173* (*STING*), stable knockdown of *STING* and *MB21D1* (*cGAS*), RNA isolation, reverse transcription, primer information, preparation of protein lysates, Western blot analysis, Western blot antibodies, RPPA, method for tumor growth assessment, *in vivo* CD8 depletion, flow cytometry antibodies, histologic analysis, micronuclei assay, and statistical methods, see Supplementary Materials and Methods.

Disclosure of Potential Conflicts of Interest

J. Sage reports receiving a commercial research grant from StemCentrx/AbbVie and has ownership interest (including stock, patents, etc.) in Forty Seven Inc. J.V. Heymach reports receiving a commercial research grant from AstraZeneca and is a consultant/advisory board member for AstraZeneca, BMS, GSK, Merck, EMD Serono, Genentech, Pfizer, Bayer, and Boerhinger Ingelheim. D.L. Gibbons reports receiving commercial research grants from AstraZeneca, Janssen Research & Development, and Takeda, and is a consultant/advisory board member for AstraZeneca, GlaxoSmithKline, Janssen R&D, and Sanofi. L.A. Byers reports receiving commercial research grants from AbbVie, AstraZeneca, and Sierra Oncology, and is a consultant/advisory board member for AstraZeneca, AbbVie, and Pharma Mar, SA. No potential conflicts of interest were disclosed by the other authors.

Authors' Contributions

Conception and design: T. Sen, J.V. Heymach, D.L. Gibbons, L.A. Byers

Development of methodology: T. Sen, L. Chen, J. Fujimoto, I.I. Wistuba, L.A. Byers

Acquisition of data (provided animals, acquired and managed patients, provided facilities, etc.): T. Sen, B.L. Rodriguez, C.M. Della Corte, N. Morikawa, J. Fujimoto, S. Cristea, T. Nguyen, Y. Fan, I.I. Wistuba, J.V. Heymach, L.A. Byers

Analysis and interpretation of data (e.g., statistical analysis, biostatistics, computational analysis): T. Sen, B.L. Rodriguez, L. Chen, C.M. Della Corte, J. Fujimoto, L. Diao, L. Li, J. Wang, J.V. Heymach, L.A. Byers

Writing, review, and/or revision of the manuscript: T. Sen, C.M. Della Corte, J. Fujimoto, L. Li, B.S. Glisson, I.I. Wistuba, J. Sage, J.V. Heymach, D.L. Gibbons, L.A. Byers

Administrative, technical, or material support (i.e., reporting or organizing data, constructing databases): T. Sen, L. Chen, J. Fujimoto, Y. Yang, D.L. Gibbons, L.A. Byers

Study supervision: T. Sen, L. Chen, J. Fujimoto, J. Sage, D.L. Gibbons, L.A. Byers

Acknowledgments

This work was supported by the NIH/NCI award U01-CA213273 (J. Sage, J.V. Heymach, L.A. Byers); NIH/NCI award R01-CA207295 (L.A. Byers); the Lung Cancer Research Foundation (T. Sen); NIH/NCI CCSG P30-CA016672 (shRNA and ORFeome Core, Bioinformatics Shared Resource); The University of Texas-Southwestern and MD Anderson Cancer Center Lung SPORE NIH/NCI award P50-CA070907 (J.V. Heymach, J. Wang, L. Chen, I.I. Wistuba, L.A. Byers); through generous philanthropic contributions to The University of Texas MD Anderson Lung Cancer Moon Shot Program (J.V. Heymach, J. Wang, L.A. Byers); The MD Anderson Cancer Center Small Cell Lung Cancer Working Group and Abell Hangar Foundation Distinguished Professor Endowment (B.S. Glisson), an MD Anderson Cancer Center Physician Scientist Award (L.A. Byers); The Rexanna Foundation for Fighting Lung Cancer (J.V. Heymach, L.A. Byers); and The Elsa U. Pardee Foundation grant (L. Chen). The authors wish to thank Dr. Robert Cardnell, Dr. Erica Goodoff (Department of Scientific Publications, MD Anderson), and Dr. Lara Carolina Alvarez de Lacerda Landry for their excellent assistance with editing the manuscript and the figures, and Dr. Emily Roarty for scientific and administrative support.

The costs of publication of this article were defrayed in part by the payment of page charges. This article must therefore be hereby marked *advertisement* in accordance with 18 U.S.C. Section 1734 solely to indicate this fact.

Received September 4, 2018; revised January 14, 2019; accepted January 30, 2019; published first February 18, 2019.

REFERENCES

1. Ribas A, Wolchok JD. Cancer immunotherapy using checkpoint blockade. Science 2018;359:1350–5.
2. Sharma P, Allison JP. The future of immune checkpoint therapy. Science 2015;348:56–61.
3. Topalian SL, Drake CG, Pardoll DM. Immune checkpoint blockade: a common denominator approach to cancer therapy. Cancer Cell 2015;27:450–61.

4. Ferris RL, Blumenschein G Jr., Fayette J, Guigay J, Colevas AD, Licitra L, et al. Nivolumab for recurrent squamous-cell carcinoma of the Head and Neck. N Engl J Med 2016;375:1856–67.
5. Reck M, Rodriguez-Abreu D, Robinson AG, Hui R, Csoszi T, Fulop A, et al. Pembrolizumab versus chemotherapy for PD-L1-positive non-small-cell lung cancer. N Engl J Med 2016;375:1823–33.
6. Robert C, Long GV, Brady B, Dutriaux C, Maio M, Mortier L, et al. Nivolumab in previously untreated melanoma without BRAF mutation. N Engl J Med 2015;372:320–30.
7. Sharma P, Hu-Lieskovan S, Wargo JA, Ribas A. Primary, adaptive, and acquired resistance to cancer immunotherapy. Cell 2017;168:707–23.
8. Hellmann MD, Callahan MK, Awad MM, Calvo E, Ascierto PA, Atmaca A, et al. Tumor mutational burden and efficacy of nivolumab monotherapy and in combination with ipilimumab in small-cell lung cancer. Cancer Cell 2018;33:853–61.e4.
9. Cheng Y, Li H, Liu Y, Ma L, Liu X, Liu Y, et al. Distribution and clinical significance of CTLA4, PD-1 and PD-L1 in peripheral blood of patients with small-cell lung cancer. J Clin Oncol 2015;33:7574.
10. Ishii H, Azuma K, Kawahara A, Yamada K, Imamura Y, Tokito T, et al. Significance of programmed cell death-ligand 1 expression and its association with survival in patients with small cell lung cancer. J Thoracic Oncol 2015;10:426–30.
11. Yamane H, Isozaki H, Takeyama M, Ochi N, Kudo K, Honda Y, et al. Programmed cell death protein 1 and programmed death-ligand 1 are expressed on the surface of some small-cell lung cancer lines. Am J Cancer Res 2015;5:1553–7.
12. Paglialunga L, Salih Z, Ricciuti B, Califano R. Immune checkpoint blockade in small cell lung cancer: is there a light at the end of the tunnel? ESMO Open 2016;1.
13. Majem M, Rudin CM. Small-cell lung cancer in the era of immunotherapy. Translational Lung Cancer Res 2017;6:S67–S70.
14. Byers LA, Wang J, Nilsson MB, Fujimoto J, Saintigny P, Yordy J, et al. Proteomic profiling identifies dysregulated pathways in small cell lung cancer and novel therapeutic targets including PARP1. Cancer Discov 2012;2:798–811.
15. Cardnell RJ, Feng Y, Diao L, Fan YH, Masrorpour F, Wang J, et al. Proteomic markers of DNA repair and PI3K pathway activation predict response to the PARP inhibitor BMN 673 in small cell lung cancer. Clin Cancer Res 2013;19:6322–8.
16. de Bono J, Ramanathan RK, Mina L, Chugh R, Glaspy J, Rafii S, et al. Phase I, dose-escalation, two-part trial of the PARP inhibitor talazoparib in patients with advanced germline BRCA1/2 mutations and selected sporadic cancers. Cancer Discov 2017;7:620–9.
17. Sen T, Tong P, Diao L, Li L, Fan Y, Hoff J, et al. Targeting AXL and mTOR pathway overcomes primary and acquired resistance to WEE1 inhibition in small-cell lung cancer. Clin Cancer Res 2017;23:6239–53.
18. Sen T, Tong P, Stewart CA, Cristea S, Valliani A, Shames DS, et al. CHK1 inhibition in small-cell lung cancer produces single-agent activity in biomarker-defined disease subsets and combination activity with cisplatin or olaparib. Cancer Res 2017;77:3870–84.
19. Pietanza MC, Waqar SN, Krug LM, Dowlati A, Hann CL, Chiappori A, et al. Randomized, double-blind, phase II study of temozolomide in combination with either veliparib or placebo in patients with relapsed-sensitive or refractory small-cell lung cancer. J Clin Oncol 2018;77:7672.
20. Sen T, Gay CM, Byers LA. Targeting DNA damage repair in small cell lung cancer and the biomarker landscape. Translat Lung Cancer Res 2018;7:50–68.
21. Chatzinikolaou G, Karakasilioti I, Garinis GA. DNA damage and innate immunity: links and trade-offs. Trends Immunol 2014;35:429–35.
22. Jiao S, Xia W, Yamaguchi H, Wei Y, Chen MK, Hsu JM, et al. PARP inhibitor upregulates PD-L1 expression and enhances cancer-associated immunosuppression. Clin Cancer Res 2017;23:3711–20.
23. Jahchan NS, Dudley JT, Mazur PK, Flores N, Yang D, Palmerton A, et al. A drug repositioning approach identifies tricyclic antidepressants as inhibitors of small cell lung cancer and other neuroendocrine tumors. Cancer Discov 2013;3:1364–77.
24. Schaffer BE, Park KS, Yiu G, Conklin JF, Lin C, Burkhart DL, et al. Loss of p130 accelerates tumor development in a mouse model for human small-cell lung carcinoma. Cancer Res 2010;70:3877–83.
25. Cardnell RJ, Feng Y, Mukherjee S, Diao L, Tong P, Stewart CA, et al. Activation of the PI3K/mTOR pathway following PARP inhibition in small cell lung cancer. PLoS One 2016;11:e0152584.
26. Li T, Chen ZJ. The cGAS–cGAMP–STING pathway connects DNA damage to inflammation, senescence, and cancer. J Exp Med 2018;215:1287–99.
27. Corrales L, McWhirter SM, Dubensky TW Jr., Gajewski TF. The host STING pathway at the interface of cancer and immunity. J Clin Invest 2016;126:2404–11.
28. Burdette DL, Monroe KM, Sotelo-Troha K, Iwig JS, Eckert B, Hyodo M, et al. STING is a direct innate immune sensor of cyclic di-GMP. Nature 2011;478:515–8.
29. Ishikawa H, Ma Z, Barber GN. STING regulates intracellular DNA-mediated, type I interferon-dependent innate immunity. Nature 2009;461:788–92.
30. Sun L, Wu J, Du F, Chen X, Chen ZJ. Cyclic GMP-AMP synthase is a cytosolic DNA sensor that activates the type I interferon pathway. Science (New York, NY) 2013;339:786–91.
31. Brzostek-Racine S, Gordon C, Van Scoy S, Reich NC. The DNA damage response induces IFN. J Immunol 2011;187:5336–45.
32. Barber GN. STING: infection, inflammation and cancer. Nat Rev Immunol 2015;15:760–70.
33. Chen Q, Sun L, Chen ZJ. Regulation and function of the cGAS–STING pathway of cytosolic DNA sensing. Nat Immunol 2016;17:1142.
34. Groom JR, Luster AD. CXCR3 in T cell function. Exp Cell Res 2011;317:620–31.
35. Kunz M, Toksoy A, Goebeler M, Engelhardt E, Brocker E, Gillitzer R. Strong expression of the lymphoattractant C-X-C chemokine Mig is associated with heavy infiltration of T cells in human malignant melanoma. J Pathol 1999;189:552–8.
36. Antonia SJ, Lopez-Martin JA, Bendell J, Ott PA, Taylor M, Eder JP, et al. Nivolumab alone and nivolumab plus ipilimumab in recurrent small-cell lung cancer (CheckMate 032): a multicentre, open-label, phase 1/2 trial. Lancet Oncol 2016;17:883–95.
37. Ott PA, Elez E, Hiret S, Kim DW, Morosky A, Saraf S, et al. Pembrolizumab in patients with extensive-stage small-cell lung cancer: results from the phase Ib KEYNOTE-028 Study. J Clin Oncol 2017;35:3823–9.
38. Wang W, Hodkinson P, McLaren F, MacKinnon A, Wallace W, Howie S, et al. Small cell lung cancer tumour cells induce regulatory T lymphocytes, and patient survival correlates negatively with FOXP3+ cells in tumour infiltrate. Int J Cancer 2012;131:E928–37.
39. Vranić S. Microsatellite instability status predicts response to anti-PD-1/PD-L1 therapy regardless the histotype: a comment on recent advances. Bosn J Basic Med Sci 2017;17:274–5.
40. Sato H, Niimi A, Yasuhara T, Permata TBM, Hagiwara Y, Isono M, et al. DNA double-strand break repair pathway regulates PD-L1 expression in cancer cells. Nature Commun 2017;8:1751.
41. George J, Lim JS, Jang SJ, Cun Y, Ozretic L, Kong G, et al. Comprehensive genomic profiles of small cell lung cancer. Nature 2015;524:47–53.
42. Parkes EE, Walker SM, Taggart LE, McCabe N, Knight LA, Wilkinson R, et al. Activation of STING-Dependent Innate Immune Signaling By S-Phase-Specific DNA damage in breast cancer. J Natl Cancer Inst 2017;109.
43. Liu Y, Li Y, Liu S, Adeegbe DO, Christensen CL, Quinn MM, et al. NK cells mediate synergistic antitumor effects of combined inhibition of HDAC6 and BET in a SCLC preclinical model. Cancer Res 2018;78:3709–17.